Data Repository Item. Analytical methods.

PETROGRAPHY. A thin section cut from sandstone breccia sample 13RE07 was first analyzed using transmitted light microscopy with a Leica DM EP petrographic microscope. This method allowed the identification of shock microstructures in quartz grains, and documentation of lithic clasts. Zircons were found to primarily occur as loose grains in the matrix, although a few were noted within clasts. The matrix is comprised of sand-sized grains of quartz and alkali feldspar, as well as fine-grained clay. Many grains are pervasively stained with a dark red-orange cement that renders many them opaque in transmitted light (Fig. DR1). Many of the clasts appear to be sedimentary in origin, consisting largely of quartz and clay; banding (layering?) is present in some. Some clasts were clay-rich and quartz-poor, while others appeared to be sandstone. No clasts could be confidently identified as igneous or metamorphic rocks; all appeared consistent with having been derived from the Mt. Simon sandstone or a lithological similar unit. No carbonate clasts were observed. The only shock microstructures identified in quartz were planar fractures (PDFs were not observed). The planar fractures are closely spaced (5-40 μm) and occur in parallel sets in different crystallographic orientations and are remarkably similar to cleavage in other minerals. Individual fractures appear to be open, and not filled with secondary material. Nearly identical planar microstructures were documented in quartz grains from samples of Rock Elm breccia by French et al. (2004) (see their Fig. 3).

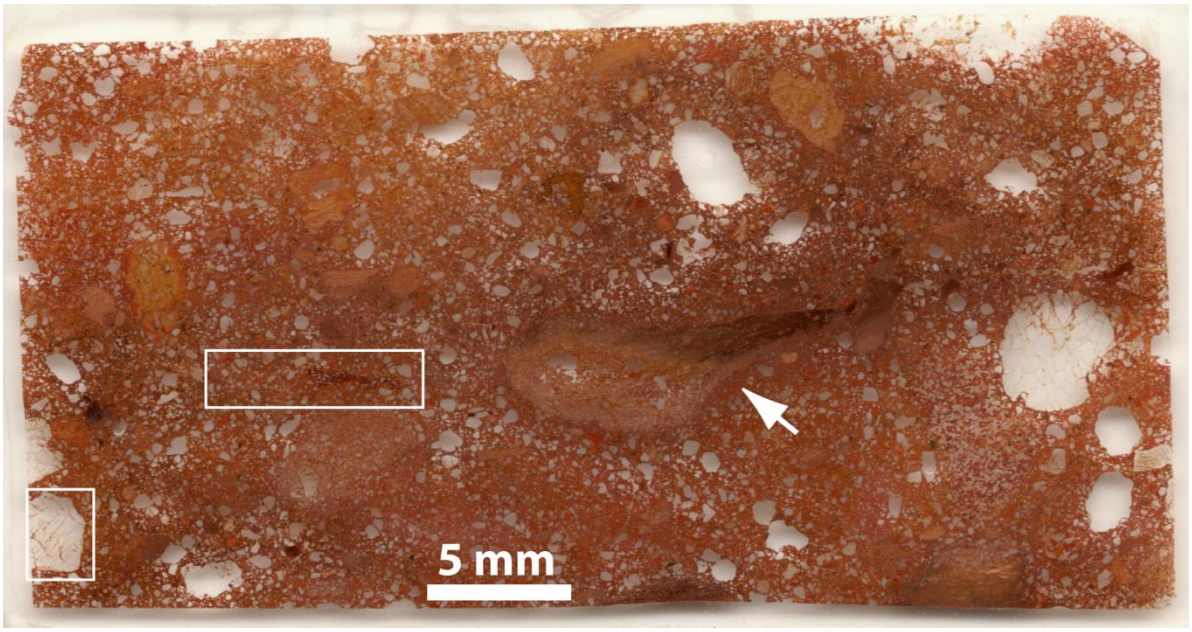

Figure DR1. Scan of the analyzed thin section (sample 13RE07). The white box along the lower-left edge of the section shows the location of the shocked quartz grain shown in Figure 1C. The larger white box to the left of center shows the region where zircons 9, 10, and 36 were found. The white arrow points to a deformed lithic clast.

SCANNING ELECTRON MICROSCOPY. The same section was analyzed using a Hitachi 3400S W-filament scanning electron microscope (SEM) at the University of Wisconsin-Madison. Standard SEM methods, including secondary electron (SE) and backscatter electron (BSE) imaging, and energy dispersive spectroscopy (EDS), were used with operating conditions of 15 kV and variable apertures.

High spatial resolution SEM analysis was conducted using a Tescan MIRA3 field emission gun (FEG) SEM at the Electron Microscopy Facility at Curtin University. The FEG-SEM was used for panchromatic cathodoluminescence (CL) imaging, and EBSD, and used SEM conditions and acquisition settings for zircon and reidite that followed closely those described in Erickson et al. (2015), and are summarized briefly here. Automated EBSD maps of regions of interest were generated by indexing of electron backscatter diffraction patterns on user-defined grids, and were collected for zircons 9, 10, and 36. Maps included both whole-grain analyses at ~0.2 μm step size and high resolution (0.05 μm step size) specific areas of interest. EBSD analyses were collected with a 20 kV accelerating voltage, 70° sample tilt, 20.5 mm working distance, and 18 nA beam intensity (Table 1). Electron backscatter patterns were collected with a Nordlys Nano high resolution detector and Oxford Instruments Aztec system using routine data acquisition and noise reduction settings (Table 1; Reddy et al., 2007). EBSD maps and pole figures were processed using the Tango and Mambo modules in the Oxford Instruments/HKL Channel 5 software package.

Grain size statistics of the nanoparticulate reidite were quantified using the Tango module in Channel5 software package of Oxford Instruments/HKL. Initially, noise reduction involved infill of isolated zero solution pixels with an average orientation based on a seven nearest neighbor extrapolation. Grains were identified automatically from a subset of the map that excluded the lamellar reidite, and was based on an orientation threshold of 10°. Only grains greater than 75 nm (i.e., 1.5 pixels) in diameter were then considered in the final statistics to remove the effects of potentially erroneous isolated data points.

REFERENCES

French, B.M., Cordua, W.S., and Plescia, J.B., 2004, The Rock Elm meteorite impact structure, Wisconsin: Geology and shock-metamorphic effects in quartz: Geological Society of America Bulletin, v. 116, p. 200–218, doi:10.1130/B25207.1.

Reddy, S.M., Timms, N.E., Pantleon, W., and Trimby, T., 2007, Quantitative characterization of plastic deformation of zircon and geological implications: Contributions to Mineralogy and Petrology v. 153, p. 625-645.

Data Repository item. EBSD analytical conditions.

EBSD analysis conditions.

SEM Model	Tescan Mira3 FEG-SEM				
Grain	Zircon 36	Zircon 9	Zircon 9	Zircon 10	Zircon 10
Show in figure	2A, DR	2B	3C, 3D	2C	DR
Acquisition speed (Hz)	22.42	22.29	22.53	40.01	21.92
Background (frames)	64	64	64	64	64
Binning	2x2	2x2	2x2	4x4	2x2
Gain	High	High	High	High	High
Hough resolution	60	60	60	60	60
Band detection min/max	6/8	6/8	6/8	6/8	6/8
Average mean angular deviation (zircon)	0.80	0.61	0.62	0.60	0.65
X steps	369	276	727	285	136
Y steps	326	247	919	270	344
Step distance (nm)	50	200	50	200	50
Noise reduction – 'wildspike'	Yes	Yes	Yes	Yes	Yes
n neighbour zero solution extrapolation	0	0	0	0	0
Kuwahara Filter	No	No	No	No	No
Tescan Mira3 FEG-SEM settings					
EBSD system	Nordlys Detector - Aztec				
Carbon coat (<5nm)	Yes	Yes	Yes	Yes	Yes
Acc. voltage (kV)	20	20	20	20	20
Working distance (mm)	20.5	20.5	20.5	20.5	20.5
Tilt (degrees)	70	70	70	70	70

DR = Data Repository

Data Repository Item. Additional images of zircon 36. A: Back-scattered electron image of zircon 36 showing variations in average atomic number. B: Map showing crystallographic misorientation across zircon 36, relative to the red cross (near bottom of grain). C: Map showing crystallographic orientation of zircon 36 (with an inverse pole figure color scheme). Twins appear as green lamellae on right side of grain. D: Pole figures for the host zircon and microtwins (labeled).

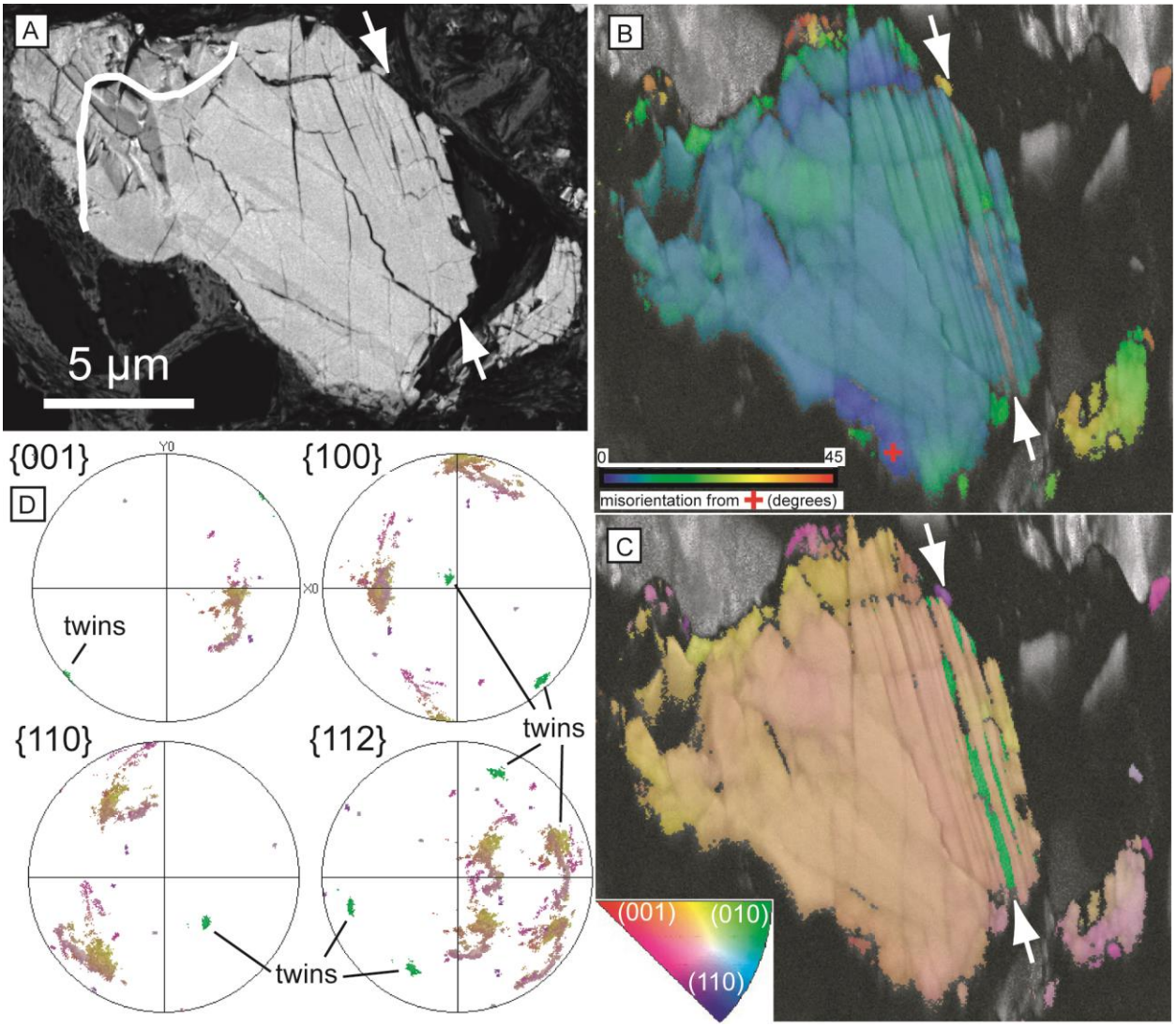

Data Repository Item. Additional images of zircon 9. A: Back-scattered electron image showing variations in average atomic number; lamellar reidite (brighter) is indicated by black arrow. B: Cathodoluminescence image showing how reidite are non-luminescent (see white arrow), and cross-cut growth zoning. The oscillatory zoned core is labeled.

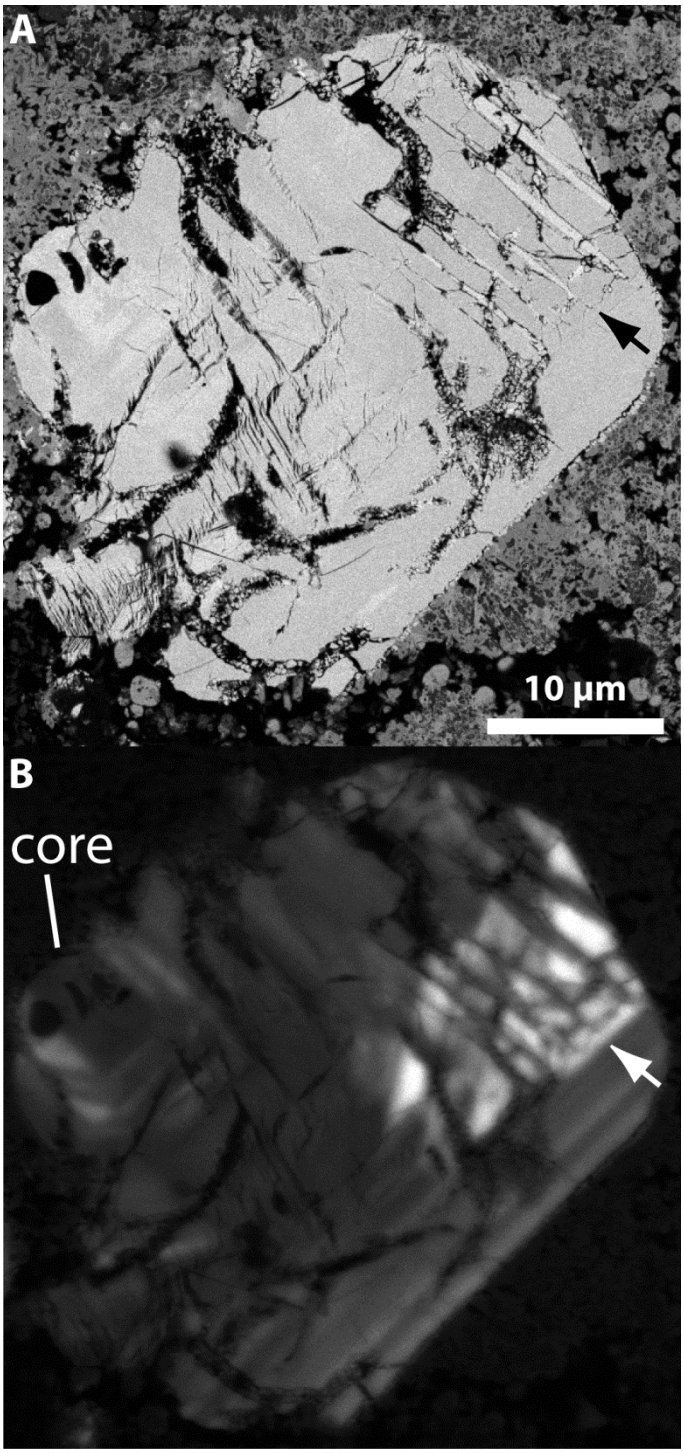

Data Repository Item. Additional images of zircon 10. A: Back-scattered electron image showing variations in average atomic number. B: CL image. C: Phase map. D: Map showing crystallographic orientation (with an inverse pole figure color scheme). E: Map showing crystallographic misorientation, relative to the red cross (near top of grain). F,G,H: Close-up maps of a reidite domain from inset in C (images as in C,D,E). I. Pole figures for the host zircon and reidite.